

# Evidential time-to-event prediction model with well-calibrated uncertainty estimation

Ling Huang<sup>a</sup>, Yucheng Xing<sup>a</sup>, Swapnil Mishra<sup>a</sup>, Thierry Denceux<sup>b,c</sup>, Mengling Feng<sup>a,d</sup>

<sup>a</sup>*Saw Swee Hock School of Public Health, National University of Singapore, Singapore,*

<sup>b</sup>*Heudiasyc, CNRS, Université de Technologie de Compiègne, France,*

<sup>c</sup>*Institut universitaire de France, Paris, France,*

<sup>d</sup>*Institute of Data Science, National University of Singapore, Singapore,*

---

## Abstract

Time-to-event analysis, or Survival analysis, provides valuable insights into clinical prognosis and treatment recommendations. However, this task is typically more challenging than other regression tasks due to the censored observations. Moreover, concerns regarding the reliability of predictions persist among clinicians, mainly attributed to the absence of confidence assessment, robustness, and calibration of prediction. To address those challenges, we introduce an evidential regression model designed especially for time-to-event prediction tasks, with which the most plausible event time, is directly quantified by aggregated Gaussian random fuzzy numbers (GRFNs). The GRFNs are a newly introduced family of random fuzzy subsets of the real line that generalizes both Gaussian random variables and Gaussian possibility distributions. Different from conventional methods that construct models based on strict data distribution, e.g., proportional hazard function, our model only assumes the event time is encoded in a real line GFRN without any strict distribution assumption, therefore offering more flexibility in complex data scenarios. Furthermore, the epistemic and aleatory uncertainty regarding the event time is quantified within the aggregated GRFN as well. Our model can, therefore, provide more detailed clinical decision-making guidance with two more degrees of information. The model is fit by minimizing a generalized negative log-likelihood function that accounts for data censoring based on uncertainty evidence reasoning. Experimental results on simulated datasets with varying data distributions and censoring scenarios, as well as on real-world datasets across diverse clinical settings and tasks, demonstrate that our model achieves both accurate and reliable performance, outperforming state-of-the-art methods.

**Keywords:** Time-to-event prediction, Data censoring, Dempster-Shafer theory, Gaussian Random Fuzzy number, Aleatory and epistemic uncertainty

---

## 1. Introduction

Time-to-event analysis, also known as survival analysis, focuses on predicting the time it takes for an event of interest to occur, such as time to death, disease recurrence, or treatment failure. Accurately predicting the event time or modeling the time-to-event functions can

provide valuable clinical insights such as risk stratification [20], or clinical decisions such as treatment planning [42] and predictive prognostic [18].

*Data censoring.* Time-to-event data often involves censoring observation, meaning that the exact event time is unknown for some data. This attribute makes the available event ground truth partially reliable and makes estimating survival probabilities difficult. Random Survival Forests (RSF) [26], a non-parametric model that builds upon the random forest algorithm and ensemble learning, shows advantages where the underlying survival distribution is complex while struggling with very high-dimensional and lacks interpretability. Cox proportional hazards model (Cox model) [5], proposed by Cox in 1972, offers a straightforward approach to handling censoring by proportional hazards (PH) assumption across covariates. The PH assumption holds that the hazard ratio (i.e., the risk of an event happening at any given time point) between two individuals is constant over time. Faraggi and Simon [15] first extended the Cox model by replacing its linear predictor with a one-hidden layer multilayer perceptron (MLP). Deep learning-based Cox models, e.g., DeepSurv [29] and Cox-CC [30], have shown promising performance recently. Despite its widespread use, the PH assumption may prove unrealistic in complex scenarios, potentially leading to biased parameter estimates and inaccurate predictions. Furthermore, the Cox model estimates the baseline hazard function solely based on observed event times, which can introduce extra biases or information loss when data is limited. Researchers, therefore, introduced more flexibility to the PH assumption, e.g., Kvamme et al. proposed a time-dependent Cox model (Cox-Time) to account for time-varying covariates [30]. While enhanced prediction accuracy, trust regarding those methods remains a main obstacle in adopting them in clinical decisions.

*Prediction uncertainty.* Prediction uncertainty, undermines clinician trust in AI models and delays their adoption in clinical workflows, posing another challenge to time-to-event analysis. High prediction uncertainty makes it difficult to tailor treatment plans, negatively impacting patient outcomes. There are two main types of uncertainty: aleatory and epistemic uncertainty. For censored datasets, the aleatory uncertainty arises from natural variability in event times, while the epistemic uncertainty is introduced by data censoring. Existing research is mostly based on Bayesian methods and quantifies uncertainty based on prediction variants with techniques such as ensembling or dropout. For example, Li et al. characterized prognostic uncertainties by calculating credible intervals using a sequential Bayesian boosting algorithm [32]; Chai et al. quantified uncertainty with Monte Carlo dropout [3]. However, those methods lack flexibility in representing and combining imperfect (e.g., uncertain, unreliable, or conflicting) evidence.

*Confidence calibration.* The third challenge of applying time-to-event models in clinical practice lies in prediction reliability. Calibration, also known as reliability in Bayesian analysis [6], is a statistical concept that refers to the consistency of estimates relative to observed measurements, and is important in high-risk tasks such as disease diagnosis [16] and tumor segmentation [34, 21]. Nevertheless, the calibration issue is relatively underexplored in time-to-event models. Early research on calibration mainly focuses on using Brier scores and negative loglikelihood, or their extensions to assess calibration performance [38, 41].

More recently, Chapfuwa et al. accounted for prediction calibration and uncertainty with a survival-function matching estimator, which estimates and compares conditional survival distributions [4]. However, most of the methods are based on probability calibration, and as [24] pointed out, probabilistic models can potentially lead to erroneous prediction calibration in complex data distribution scenarios.

*Study problem and proposals.* In this study <sup>1</sup>, we investigate whether time-to-event prediction can be accurate, well-calibrated, and clinically applicable via evidence-based uncertainty quantification and information fusion. We propose an evidential time-to-event prediction model that does not rely on specific forms of distribution assumptions, e.g., the conventional PH assumption. Instead, we calculate the evidence of a time interval directly under the framework of belief functions [7, 36] and random fuzzy sets [8, 12]. The proposed approach modifies the Gaussian random fuzzy numbers (GRFNs)-based regression model introduced in [9, 11] to account for data censoring with a generalized negative log-likelihood optimization function. GRFNs are a newly introduced family of random fuzzy subsets of the real line, which can be further studied to analyze the reliability of the prediction results. In addition to outputting the most plausible event time, our model outputs two additional quantities: standard deviation and precision measuring, respectively, aleatory and epistemic prediction uncertainties. To our best knowledge, this is the first work involving a regression model that can predict the most plausible event time with both aleatory and epistemic uncertainty provided in the presence of data censoring. Moreover, the quantified precision allows us to compute conservative prediction intervals with specified belief degrees with confidence calibration. The model is fitted by minimizing the generalized negative log-likelihood loss function with censored and uncensored data optimized independently using different forms of evidence at event time.

The rest of this paper is organized as follows. Necessary notions about time-to-event analysis and GRFNs are first recalled in Section 2. Our approach is then introduced in Section 3, and experimental results are reported in Section 4. Finally, Section 5 concludes the paper and presents some directions for further research.

## 2. Background

The basic concepts of time-to-event analysis are first recalled in Section 2.1. The Gaussian random fuzzy number and its extensions are then introduced in Sections 2.2.

### 2.1. Time-to-event analysis

In time-to-event analysis, the actual event time of an individual can be regarded as the observed value of a variable,  $T, T > 0$ . We call  $T$  the random variable associated with the survival time. Suppose this random variable has a probability distribution with underlying

---

<sup>1</sup>This paper is an extended version of the short paper presented at the 8th International Conference on Belief Functions (BELIEF 2024) [25].

probability density function  $f(t|x)$ , where  $x$  is the vector of covariates. The cumulative density function of  $T$  is then given by

$$F(t|x) = P(T \leq t|x) = \int_0^t f(s|x)ds, \quad (1)$$

and represents the probability that the survival time is less than some value  $t$ .

*Time to-event function.* Time to-event function, called Survival function as well, is used to identify the probability that an event will happen past time  $t$  where  $x$  is the vector of covariates with the definition

$$S(t|x) = P(T \geq t|x) = 1 - F(t|x), \quad (2)$$

$S(t)$  can also be interpreted as the chance that an individual is still alive after time  $t$  in the medical domain.

*Hazard function.* Hazard function is widely used to express the risk of an event such as a death occurring at some time  $t$ . In other words, the hazard function describes the ‘intensity of death’ at time  $t$  given that the individual has already survived past time  $t$ . Consider the probability that the random variable associated with an individual’s survival time,  $T$ , lies between  $t$  and  $t + \Delta t$ , conditional on  $T$  being greater than or equal to  $t$ , written  $P(t + \Delta t | T \geq t)$ . This conditional probability is then expressed as a probability per unit time by dividing by the time interval,  $\Delta t$ , to give a rate. The hazard function,  $h(t|x)$ , is then defined as

$$h(t|x) = \lim_{\Delta t \rightarrow 0} \frac{P(t \leq T < t + \Delta t | T \geq t; x)}{\Delta t} = \frac{f(t|x)}{S(t|x)}, \quad (3)$$

where  $f(t|x) = \frac{d}{dt}F(t|x)$  is the probability density function of a random variable  $T$ . If we can model the hazard function, the cumulative amount of hazard up to time  $t$  is defined as

$$H(t|x) = \int_0^t h(s|x)ds, \quad (4)$$

and the survival function can also be constructed through the cumulative hazard function

$$S(t|x) = \exp(-H(t|x)). \quad (5)$$

*Data censoring.* In real-life scenarios, the true event times may be unknown for some individuals. This can occur when the follow-up time for an individual is not enough for the event to happen, or an individual may quit the study before its termination, or there is imprecision in data collection. Instead of observing the true event time  $T$ , we then observe a possibly right-censored event time  $T^*$ , with  $T^* = \min\{T, C\}$ , where  $C$  is the censoring time. In addition, we observe the indicator  $D = \mathbb{1}\{T = T^*\}$  labeling the observed event time  $T$  as an event that happened or a censored observation.

*Full likelihood optimization.* Denoting individuals by  $i$ , with covariates  $x_i$  and observed duration  $T_i$ , the likelihood for partially censored survival times is given by

$$L(\theta) = \prod_i f(T_i | x_i)^{D_i} S(T_i | x_i)^{1-D_i}, \quad (6)$$

If  $f(T_i | x_i)$  is available,  $S(T_i | x_i)$  can be calculated with Eq 1 and Eq 2, and the survival model can be optimized by maximizing a  $L(\theta)$  related function. However, due to data censoring,  $f(T_i | x_i)$  can not be identified easily.

*Partial likelihood optimization.* For Cox-PH models, researchers often optimize the partial likelihood rather than the full likelihood as follows:

$$L(\beta) = \prod_{i=1}^n \frac{e^{\beta^T x_i}}{\sum_{j \in R(T_i)} e^{\beta^T x_j}}, \quad (7)$$

where  $R(T_i)$  is the risk set (the set of individuals still at risk just before time  $T_i$ ), and  $h(t|x) = h_0(t)e^{\beta^T x_i}$ ,  $h_0(x)$  is the baseline hazard function be left unspecified during the estimation process. Once  $\beta$  is estimated,  $h_0(t)$  can be estimated based on available data using methods such as Kaplan-Meier [28] or Breslow Estimator [2].

## 2.2. Gaussian random fuzzy number

The Dempster-Shafer (DS) theory of evidence, called belief function theory as well, [7, 36] is a framework for modeling, reasoning with, and combining imperfect information. Most applications of the DS theory consider belief functions on finite frames of discernment [39, 33, 37, 23]. This is due to the lack of practical belief function models that can handle continuous variables while remaining compatible with Dempster's rule of combination. Recently, the epistemic random fuzzy set (ERFS) theory [8, 12, 10, 14, 13] introduced by Denoeux makes it possible to overcome this limitation. ERFS is an extension of DS theory and possibility theory [40]. In this new theoretical framework, uncertain and/or fuzzy pieces of evidence are represented by random fuzzy sets inducing belief functions, and independent items of evidence are combined by the product-intersection rule generalizing both Dempster's rule and the normalized product-intersection operator of possibility theory. Based on ERFS, Denoeux introduced a practical model of a random fuzzy subset of the real line, called Gaussian random fuzzy numbers (GRFNs).

*Gaussian fuzzy numbers (GFNs).* Before introducing GRFNs, it is necessary to introduce the definition of Gaussian fuzzy numbers (GFNs). A GFN is a fuzzy subset of  $\mathbb{R}$  with the membership function

$$\Phi(t; m, h) = \exp\left(-\frac{h}{2}(t - m)^2\right), \quad (8)$$

where  $m \in \mathbb{R}$  is the mode and  $h \in [0, +\infty]$  is the precision, denoted by  $GFN(m, h)$ . A cheering property of GFN is that it is closed with respect to the normalized product

intersection: given two GFNs,  $GFN_1(m_1, h_1)$  and  $GFN_2(m_2, h_2)$ , their combination yields the new  $GFN_{12}(m_{12}, h_{12})$  with

$$m_{12} = \frac{h_1 m_1 + h_2 m_2}{h_1 + h_2} \quad (9)$$

and

$$h_{12} = h_1 + h_2. \quad (10)$$

*Gaussian random fuzzy numbers (GRFNs).* A GRFN can be defined as a GFN whose mode is a Gaussian random variable (GRV). Let  $(\omega, \sum_{\Omega}, P)$  be a probability space and  $G : \Omega \rightarrow \mathbb{R}$  be a GRV with mean  $\mu$  and variance  $\sigma^2$ . The random fuzzy set  $\tilde{X} \rightarrow [0, 1]^{\mathbb{R}}$  with the definition

$$\tilde{T}(\omega) = GFN(G(\omega), h) \quad (11)$$

is called a GRFN with mean  $\mu$ , variance  $\sigma$  and precision  $h$ , denoted by  $\tilde{T} \sim \tilde{N}(\mu, \sigma^2, h)$ . We can also say that a GRFN is defined by a location parameter  $\mu$  and two parameters  $\sigma^2$  and  $h$  corresponding, respectively, to aleatory and epistemic uncertainty. According to Eqs 9 and 10, the fused results of two GRFNs can be written as  $\tilde{T}_1 \boxplus \tilde{T}_2 \sim N(\mu_{12}, \sigma_{12}^2, h_{12})$  with

$$\mu_{12} = \frac{h_1 \mu_1 + h_2 \mu_2}{h_1 + h_2}, \quad (12a)$$

$$\sigma_{12}^2 = \frac{h_1^2 \sigma_1^2 + h_2^2 \sigma_2^2}{(h_1 + h_2)^2}, \quad (12b)$$

and

$$h_{12} = h_1 + h_2. \quad (13)$$

GRFNs are valuable for estimating uncertain information in regression tasks. This stems from their capability to be easily combined using the generalized product-intersection rule introduced in [11]. Based on the cheering capability, the author further proposed a neural network called ENNreg, which, for an observed input vector  $X = x$ , the network computes a GRFN  $\tilde{T}(x)$ , with associated belief function  $Bel_{\tilde{T}(x)}$  quantifying the uncertainty on  $\tilde{T}$  given  $x$  based on prototypes.

*Lognormal random fuzzy numbers.* A GRFN is a model of uncertainty about a variable taking values in the whole real line. In contrast, in time-to-event analysis, the response variable is always positive. The event prediction and its corresponding uncertainty in such tasks are better represented by a lognormal random fuzzy number as introduced in [10].

Let  $\psi$  be a one-to-one mapping from  $\mathbb{R}$  to a subset  $\Lambda \subseteq \mathbb{R}$ . Its extension  $\tilde{\psi}$  maps each fuzzy subset  $\tilde{F}$  of  $\mathbb{R}$  to a fuzzy subset  $\tilde{\psi}(\tilde{F})$  of  $\Lambda$  with membership function  $\lambda \mapsto \tilde{F}[\psi^{-1}(\lambda)]$ . Let  $[0, 1]^{\mathbb{R}}$  denote the set of all fuzzy subsets of  $\mathbb{R}$ , and  $\tilde{Y} : \Omega \rightarrow [0, 1]^{\mathbb{R}}$  be a RFS. By composing  $\tilde{\psi}$  with  $\tilde{Y}$ , we obtain a new RFS  $\tilde{\psi} \circ \tilde{Y} : \Omega \rightarrow [0, 1]^{\Lambda}$ . For any event  $C \subseteq \Lambda$ , we have

$$Bel_{\tilde{\psi} \circ \tilde{Y}}(C) = Bel_{\tilde{Y}}(\psi^{-1}(C)) \quad \text{and} \quad Pl_{\tilde{\psi} \circ \tilde{Y}}(C) = Pl_{\tilde{Y}}(\psi^{-1}(C)). \quad (14)$$

Taking  $\tilde{Y} \sim \tilde{N}(\mu, \sigma^2, h)$ ,  $\Lambda = [0, +\infty)$  and  $\psi = \exp$ , we obtain a *lognormal random fuzzy number*  $\tilde{T} : \widetilde{\exp} \circ \tilde{Y}$  denoted by  $\tilde{T} \sim T\tilde{N}(\mu, \sigma^2, h, \log)$ . We can remark that  $\widetilde{\log} \circ \tilde{Y} \sim \tilde{N}(\mu, \sigma^2, h)$ . Degrees of belief  $Bel_{\tilde{T}}(C)$  and  $Pl_{\tilde{T}}(C)$  for any interval  $C \subseteq [0, +\infty)$  can easily be computed from (14) and formulas given in [12] for GRFNs.

*Beleif, plausibility and contour functions regarding GRFNs*. Details regarding the calculations of the belief and plausibility function of any time interval  $[t_1, t_2]$  induced by a GRFN  $\tilde{T} \sim \tilde{N}(\mu, \sigma^2, h)$  are given in [12]. In particular, the contour function of  $\tilde{T}$  at time  $t$  is given by

$$pl_{\tilde{T}}(t) = \frac{1}{\sqrt{1+h\sigma^2}} \exp\left(-\frac{h(t-\mu)^2}{2(1+h\sigma^2)}\right). \quad (15)$$

For any interval  $[t_1, t_2]$ , the degree of belief on  $[t_1, t_2]$  induced by the GRFN  $\tilde{T}$  are,

$$\begin{aligned} Bel_{\tilde{T}}([t_1, t_2]) = & \Phi\left(\frac{t_2 - \mu}{\sigma}\right) - \Phi\left(\frac{t_1 - \mu}{\sigma}\right) \\ & - pl_{\tilde{T}}(t_1) \left[ \Phi\left(\frac{(t_1 + t_2)/2 - \mu}{\sigma\sqrt{h\sigma^2 + 1}}\right) - \Phi\left(\frac{t_1 - \mu}{\sigma\sqrt{h\sigma^2 + 1}}\right) \right] \\ & - pl_{\tilde{T}}(t_2) \left[ \Phi\left(\frac{t_2 - \mu}{\sigma\sqrt{h\sigma^2 + 1}}\right) - \Phi\left(\frac{(t_1 + t_2)/2 - \mu}{\sigma\sqrt{h\sigma^2 + 1}}\right) \right] \end{aligned} \quad (16)$$

and the plausibility on  $[t_1, t_2]$  induced by the GRFN  $\tilde{T} \sim \tilde{N}$  are,

$$\begin{aligned} Pl_{\tilde{T}}([t_1, t_2]) = & \Phi\left(\frac{t_2 - \mu}{\sigma}\right) - \Phi\left(\frac{t_1 - \mu}{\sigma}\right) \\ & + pl_{\tilde{T}}(t_1) \left[ \Phi\left(\frac{t_1 - \mu}{\sigma\sqrt{h\sigma^2 + 1}}\right) \right] \\ & + pl_{\tilde{T}}(t_2) \left[ 1 - \Phi\left(\frac{t_2 - \mu}{\sigma\sqrt{h\sigma^2 + 1}}\right) \right]. \end{aligned} \quad (17)$$

The lower and upper cdfs of  $Bel$  and  $Pl$  have the following expressions:

$$Bel_{\tilde{T}}((-\infty, t]) = \Phi\left(\frac{t - \mu}{\sigma}\right) - pl_{\tilde{T}}(t) \Phi\left(-\frac{t - \mu}{\sigma\sqrt{1+h\sigma^2}}\right), \quad (18)$$

where  $\Phi$  is the standard normal cdf, and

$$Pl_{\tilde{T}}((-\infty, t]) = Bel_{\tilde{T}}((-\infty, t]) + pl_{\tilde{T}}(t). \quad (19)$$

### 3. Proposed methods

#### 3.1. Study overview

Figure 1 shows the overview of this study. The time-to-event prediction framework consists of data representation, evidence modeling, and evidence fusion. Data representation

encodes tabular data into distance-related features induced by distribution prototypes. Evidence modeling then maps these features to GRFNs, which are then combined in the evidence fusion layer later. The optimization of the framework is based on the generalized negative log-likelihood considering two conditions: censored and uncensored observations. The optimized model predicts three dimensions of information: the most plausible event time, the aleatory, and the epistemic uncertainty regarding the predicted time. The evaluation of the framework includes both quantitative analysis (i.e., censoring rate, data distribution, and clinical tasks) and qualitative analysis (i.e., prediction and uncertainty visualization, heatmaps, reliability diagrams, and survival curves).

### 3.2. Evidential survival prediction

To predict event time in the real line, we adopt the approach introduced in [11] and construct a GRFN-based evidential neural network, named *ENNreg* to predict  $Y = \log(T)$ , where  $T$  is the time to event. With ENNreg, the underlying pieces of evidence of event time from input data can be represented as the evidence for the corresponding plausible random fuzzy sets (GRFNs) obtained from the distances between input  $x$  and the distribution prototypes, and then the random fuzzy sets are combined by the extension of Dempster's combination rule, denoted by  $\boxplus$ , for the most plausible random fuzzy set. ENNreg is composed of three layers: the distance layer, the evidence mapping layer, and the fusion layer.

*Distance calculation.* Let  $p_1, \dots, p_K$  denote  $K$  vectors in the  $p$ -dimensional feature space, called prototypes. For each prototype  $p_k$ , the activated distance between input covariant  $x$  and prototype  $p_k$  is measured by

$$s_k(x) = \exp(-\gamma_k^2 |x - p_k|^2), \quad (20)$$

where  $\gamma$  is a positive scale parameter.

*Evidence mapping.* In the evidence mapping layer, the evidence of prototype  $p_k$  is then represented by a GRFN  $\log(\tilde{T}_k(x)) \sim \tilde{N}(\mu_k(x), \sigma_k^2, s_k(x)h_k)$ . Parameter  $\mu_k(x)$  is the mean of GRFN with the definition

$$\mu_k(x) = \beta_k^T x + \beta_{k0}, \quad (21)$$

where  $\beta_k$  is a  $p$ -dimensional vector of coefficients, and  $\beta_{k0}$  is a scalar parameter. The quantity  $\mu_k(x)$  and  $\sigma_k^2$  can be seen as an estimation of the conditional expectation and variance, respectively, of the response  $\log(\tilde{T}_k(x))$  given that  $x$  is close to  $p_k$ ;  $h_k$  is the precision.

*Evidence fusion.* The evidence fusion layer combines evidence from the  $K$  prototypes using the unnormalized product-intersection combination rule  $\boxplus$  [12] and outputs a final GRFN  $\tilde{Y}(x) \sim \tilde{N}(\mu(x), \sigma^2(x), h(x))$  given by

$$\mu(x) = \frac{\sum_{k=1}^K s_k(x) h_k \mu_k(x)}{\sum_{k=1}^K s_k(x) h_k}, \quad (22)$$

$$\sigma^2(x) = \frac{\sum_{k=1}^K s_k^2(x) h_k^2 \sigma_k^2}{(\sum_{k=1}^K s_k(x) h_k)^2}, \quad (23)$$



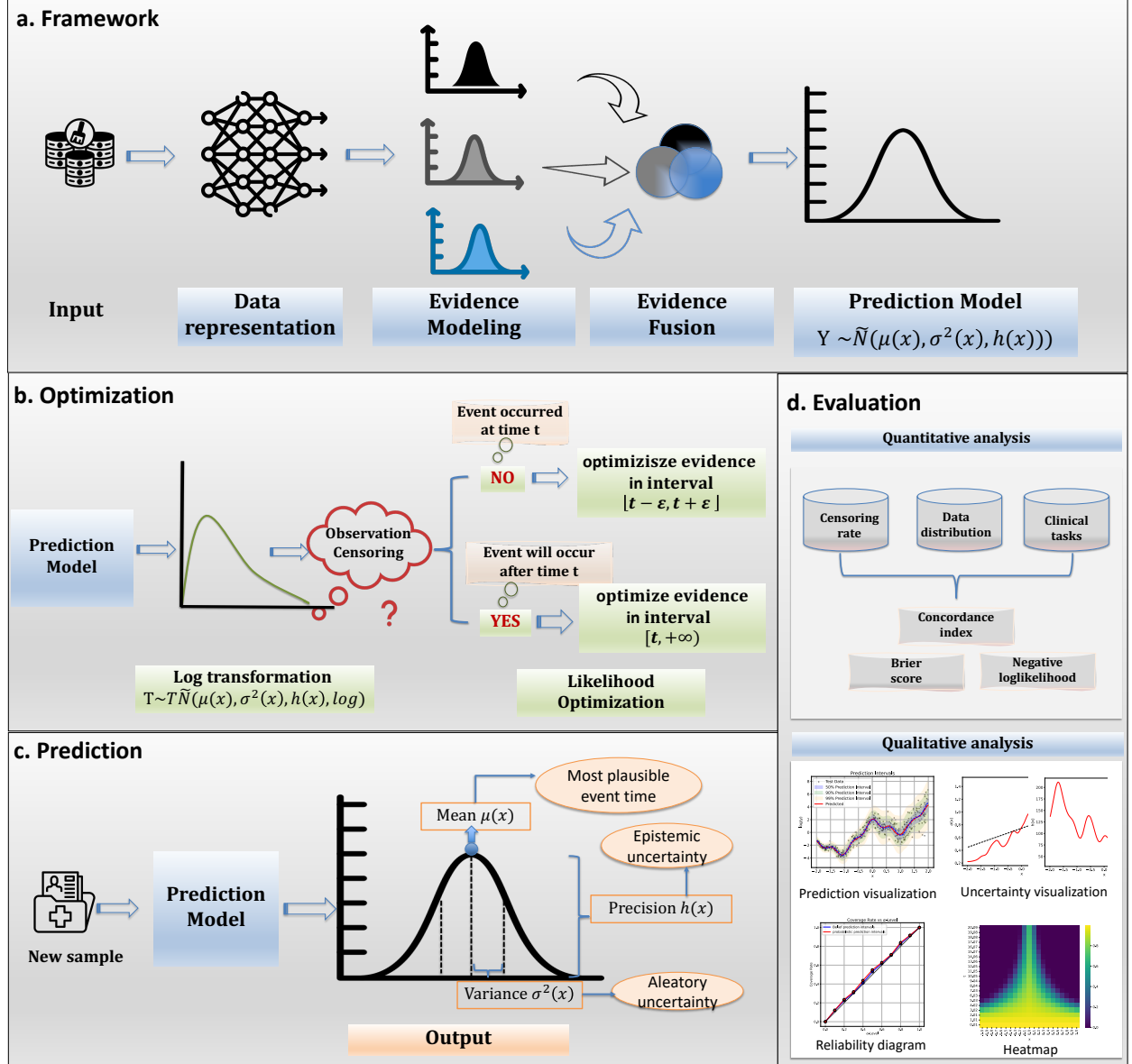


Figure 1: Overview of the study. **a. Overall framework:** consists of data representation, evidence modeling, and evidence fusion. **b. Framework optimization:** based on the generalized negative log-likelihood considering two conditions: censored and uncensored observations. **c. Framework prediction:** the model will predict three dimensions of information: the most plausible event time, the aleatory, and the epistemic uncertainty regarding the predicted time. **d. Performance evaluation:** includes both quantitative analysis (i.e., censoring rate, data distribution, and clinical tasks) and qualitative analysis (i.e., visualized prediction and uncertainty diagrams, reliability diagrams, and survival heatmaps).

and

$$h(x) = \sum_{k=1}^K s_k(x) h_k. \quad (24)$$

Here  $\mu(x)$  denotes the most plausible time-to-event prediction. The variance output  $\sigma^2(x)$  estimates the conditional variance of  $y$  given the input  $x$ , reflecting aleatory uncertainty (larger  $\sigma^2(x)$  indicates more uncertainty). In contrast, the precision output  $h(x)$  gets smaller and tends to zero when the distance to distribution prototypes increases, indicating epistemic uncertainty (smaller  $h(x)$  signifies more uncertainty). Therefore, uncertainty about  $T$  is then described by the lognormal random fuzzy number  $\tilde{T} \sim T\tilde{N}(\mu(x), \sigma^2(x), h(x), \log)$ .

### 3.3. Optimization with data censoring

Let  $\tilde{Y}$  be the output GRFN,  $y = \log(t)$  the observation, and  $D$  a binary censoring variable such that  $D = 1$  if  $\tilde{Y} = y$ , and  $D = 0$  if it is only known that  $\tilde{Y} \geq y$ . To optimize the proposed framework, we extended the negative log-likelihood loss function defined in [11] and adapted it to account for both uncensored and censored data by optimizing the evidence in two situations:

- If the data is not censored, the continuous event time  $\tilde{Y}$  is always observed with finite precision. Therefore, instead of observing an exact value, we actually observe an interval  $[y]_\epsilon = [y - \epsilon, y + \epsilon]$  centered at  $y$ . Our prediction evidence can, therefore, be characterized by either the belief function  $Bel([y]_\epsilon)$  or the plausibility function  $Pl([y]_\epsilon)$ .
- If the data is censored, the event time  $\tilde{Y}$  will only be observed in interval  $[y, \infty)$ . Our prediction evidence can now be represented as the belief function  $Bel([y, \infty))$  or plausibility function  $Pl([y, \infty))$ .

We, therefore, consider the following weighted likelihood sum of  $L_{Bel}$  or  $L_{Pl}$

$$\mathcal{L}_{\lambda, \epsilon}(\tilde{Y}, y, D) = \lambda \bar{\mathcal{L}}(\tilde{Y}, y, D) + (1 - \lambda) \underline{\mathcal{L}}(\tilde{Y}, y, D),$$

with

$$\bar{\mathcal{L}}(\tilde{Y}, y, D) = -D \ln Bel_{\tilde{Y}}([y - \epsilon, y + \epsilon]) - (1 - D) \ln Bel_{\tilde{Y}}([y, \infty)),$$

and

$$\underline{\mathcal{L}}(\tilde{Y}, y, D) = -D \ln Pl_{\tilde{Y}}([y - \epsilon, y + \epsilon]) - (1 - D) \ln Pl_{\tilde{Y}}([y, \infty)),$$

where  $\lambda$  is the hyperparameter that controls the cautiousness of the prediction (the smaller, the more cautious).

The network is trained by minimizing the regularized average loss:

$$C_{\lambda, \epsilon, \xi, \rho}^{(R)}(\Psi) = \frac{1}{n} \sum_{i=1}^n \mathcal{L}_{\lambda, \epsilon}(\tilde{Y}(x_i; \Psi), y_i, D_i) + \frac{\xi}{K} \sum_{k=1}^K h_k + \frac{\rho}{K} \sum_{k=1}^K \gamma_k^2,$$

where  $\Psi$  is the vector of all parameters,  $\tilde{Y}(x_i; \Psi)$  is the network output for input  $x_i$ ,  $\xi$  and  $\rho$  are two regularization parameters. It should be noted that the prototypes we mentioned

in (20) are included as the parameters of the network and for optimization as well. The first regularizer term  $\xi$  reduces the impact of prototypes used for prediction, for example, setting  $h_k = 0$  to discarding prototype  $k$ . The second regularizer term  $\rho$  shrinks the solution towards a linear model, for example, setting  $\gamma_k = 0$  for all  $k$  yields a linear model.

## 4. Experimental and results

In this section, the proposed framework described in Section 3 is first studied with one illustrated example to test its robustness to data censoring and, then studied in three simulated survival datasets to test its robustness to data distribution and, lastly validated on cancer and ICU datasets to test its applicability in real-world settings. The experimental settings regarding the dataset introduction, the network parameter and learning, and the evaluation criteria are first described in Section 4.1. The results on the mentioned datasets are then reported in Sections 4.2, 4.3 and 4.4.

### 4.1. Experimental setting

#### 4.1.1. Dataset

*Illustration dataset.* The illustration dataset is constructed with the following distribution: the input  $X$  has a uniform distribution in the interval  $[-2, 2]$ , and the response is

$$T = \exp \left[ 1.5X + 2 \cos(3X)^3 + \frac{X^2 + 5}{3\sqrt{5}}V \right], \quad (25)$$

where  $V \sim N(0, 1)$  is a standard normal random variable. Two elements were incorporated to simulate data censoring scenarios: the event censoring state indicator  $D$  and a random censoring time  $C$ . The censored samples are randomly selected with a probability  $p$  and assigned with  $D = 1$ , and the uncensored samples are left with  $D = 0$ . The censoring time is drawn from a uniform distribution between 0 and the maximum value in the event time  $T$ . For each censored sample, the event time  $C$  is set to the minimum of the original time value and the randomly generated censor time. Finally, a dataset with 2000 samples was generated, with 1600 samples used for training and 400 left for testing, with the censoring rate set as 0, 50%, and 90%, respectively.

*Simulated survival datasets.* Following [29], we generate patient's death time  $T$  as a function of their covariates by using the exponential Cox model:

$$T \sim \text{Exp}(\lambda(t; x)) = \text{Exp}(\lambda_0 \cdot e^{h(x)}). \quad (26)$$

Each observation  $x$  represents a patient vector with 10 covariates. The ten variables are each drawn from a uniform distribution on  $[-1, 1]$ . In both experiments, the log-risk function  $h(x)$  only depends on two of the ten covariates. This allows us to verify that ENNreg discerns the relevant covariates from the noise. We then choose a censoring time to represent the 'end of study' such that 50% of the patients have an observed event,  $D = 1$ , in the dataset. Three data distribution situations, i.e., linear proportional hazards (LPH), nonlinear (gaussian) proportional hazards (NLPH), and nonlinear nonproportional hazards (NLNPH) are considered:

Dataset	Size	Covariates	Duration(days)		Censor rate
			Min	Max	
METABRIC	1,904	9	0	355	0.42
GBSG	2,232	7	0.2	87	0.43
SUPPORT	8,873	14	2	2029	0.32

Table 1: Summary of the four data sets used in the experiments

- **Linear assumption.** Following [29], we simulate patients to have a linear  $h(x)$  so that the linear proportional hazards assumption holds true:

$$h(x) = x_0 + 2x_1. \quad (27)$$

- **Nonlinear assumption.** We set the  $h(x)$  to be nonlinear, i.e., a Gaussian function with  $\lambda_{max} = 5.0$  and a scale factor of  $r = 0.5$  [29]:

$$h(x) = \log(\lambda_{max}) \exp\left(-\frac{x_0^2 + x_1^2}{2r^2}\right) \quad (28)$$

- **Nonlinear nonproportional assumption.** The proportionality assumption of the Cox model can be rather restrictive. We, therefore, follow [30] to construct a dataset that holds the nonlinear nonproportional hazard assumption with

$$\lambda(t; x) = \lambda_0(t) \exp[g(t, x)], \quad (29)$$

where  $g(t, x)$  is a time-dependent function and  $\lambda_0$  is set to 0.02. More details about the setting of  $g(t, x)$  can be found in [29].

For LPH and NLPH datasets, 5000 samples are generated. For the NLNPH dataset, 25,000 samples are generated since the distribution is more complex.

*Real-world survival datasets.* We base the real-world validation on three survival datasets provided by [30] and [29], as they are made available through the Pycox python package<sup>2</sup> and need no further preprocessing. The data sets include the Study to Understand Prognoses Preferences Outcomes and Risks of Treatment (SUPPORT), the Molecular Taxonomy of Breast Cancer International Consortium (METABRIC), and the Rotterdam Tumor Bank and German Breast Cancer Study Group (Rot. & GBSG), shows in Table 1. A more detailed description of the four datasets can be found in [30].

---

<sup>2</sup><https://github.com/havakv/pycox>

*ICU dataset.* In addition to survival prediction, we are also interested in the prediction of ICU length of stay. We include a novel large-scale survival analysis benchmark dataset from the publicly available MIMIC-IV database [27]. The MIMIC-IV dataset contains detailed information such as vital signs, laboratory test results, medications, clinical notes, imaging reports, and demographic details. For the MIMIC-IV dataset, we extracted 24 features based on the first 24-hour clinical data following [35]. The hospital length of stay is regarded as the event time. The event of interest is defined as the mortality after admission. The event time is observed if there is a record of death in the database; otherwise, the censored time is defined as the last time of being discharged from the hospital. Samples with more than 50% missing variables are discarded directly, and multiple imputation is used to handle missing data.

#### 4.1.2. Parameter initialization

For all methods, except Cox, we used the implementation in the Python package 'Pycox'. For Cox, we used the implementation in the Python package 'lifelines'<sup>3</sup>. For ENNreg, the number of prototypes was fixed to  $K = 40$  for all datasets. For compared methods, hyperparameters were fixed according to the suggestions in their original paper. For ENNreg,  $\epsilon = 1e^{-4}\sigma_Y$  (where  $\sigma_Y$  is the estimated standard deviation of the response variable) for all the simulations. Hyperparameters  $\xi$  and  $\rho$  were fixed to 0 according to the R package 'evreg'<sup>4</sup>. The value of hyperparameter  $\lambda$  was tuned by five-fold cross-validation.

#### 4.1.3. Learning algorithm

Each model was trained on the learning set with 500 epochs using the Adam optimization algorithm. The initial learning rate was set to  $10^{-1}$ . An adjusted learning rate schedule was applied by reducing the learning rate when the training loss did not decrease in 100 epochs. An early stop mechanism was applied when the validation performance did not improve in 20 training epochs. The model with the best performance on the validation set was saved as the final model for testing. Each dataset was randomly split into training, validation, and test sets, containing 60%, 20%, and 20% of the observations, respectively. These random splits were repeated five times. Finally, the mean prediction and the 95% confidence interval were calculated and reported. All methods were implemented in Python and were trained and tested on a 2023 Apple M2 Pro with a 12-core CPU and 19-core GPU, 32 GB CPU memory.

#### 4.1.4. Evaluation criteria

Evaluation criteria for time-to-event prediction involve assessing how well a model predicts time-to-event outcomes and how effectively it handles censored data. *Concordance Index* ( $C_{idx}$ ) is one of the most common criteria that measures how well the model can correctly predict the order of events [19]. Since the  $C_{idx}$  depends only on the ordering of the predictions, it enables us to use the relative risk function instead of a metric for predicting

---

<sup>3</sup><https://lifelines.readthedocs.io/en/latest/>

<sup>4</sup><https://cran.r-project.org/web/packages/evreg/index.html>

survival time, which, therefore, is beneficial for methods that evaluate the performance of proportional hazard models. Antolini et al. proposed a time-dependent  $C_{idx}$  [1] evaluation criteria with

$$C_{idx} = P\{S(T_i | x_i) < S(T_i | x_j) \mid T_i < T_j, D_i = 1\}, \quad (30)$$

which is more flexible. Moreover, to account for tied event times and survival estimates, the authors make the modifications listed by Ishwaran et al [26] to ensure that predictions independent of  $x$ ,  $\hat{S}(t|x) = \hat{S}(t)$ , yields  $C_{idx} = 0.5$  for unique event times. In this paper, we choose time-dependent  $C_{idx}$  to evaluate how well our model predicts the ordering of patients' death times.

*Brier Score* is a common metric of the calibration of a model's prediction. To get binary value from time-to-event data, we choose a fixed time  $t$  and label data according to whether or not an observation's event time is shorter or longer than  $t$ . In [17], Graf et al. generalized the Brier score to account for censoring by weighting the scores by the inverse censoring distribution,

$$BS(t) = \frac{1}{N} \sum_1^N \left[ \frac{\hat{S}(t|x_i)^2 \mathbb{1}\{T_i \leq t, D_i = 1\}}{\hat{G}(T_i)} + \frac{(1 - \hat{S}(t|x_i))^2 \mathbb{1}\{T_i > t\}}{\hat{G}(t)} \right], \quad (31)$$

where  $N$  is the number of observations,  $\hat{G}(t)$  is the Kaplan-Meier estimate of the censoring survival function. The BS can be extended from a single duration  $t$  to an interval by computing the integrated Brier score using

$$IBS = \frac{1}{t_2 - t_1} \int_{t_1}^{t_2} BS(s) ds. \quad (32)$$

In practice, we approximate this integral by numerical integration and let the time span be the duration of the test set. We follow the suggestion in [30] to use 100 grid points to obtain stable scores.

*Binomial Log-Likelihood* is another commonly used metric in regression tasks that measures the calibration of the estimations. Using the same inverse censoring weighting as for the Brier score, we can apply this metric to censored duration time data,

$$BLL(t) = \frac{1}{N} \sum_{i=1}^N \left[ \frac{\log[1 - \hat{S}(t|x_i)] \mathbb{1}\{T_i \leq t, D_i = 1\}}{\hat{G}(T_i)} + \frac{\log[\hat{S}(t|x_i)] \mathbb{1}\{T_i > t\}}{\hat{G}(t)} \right]. \quad (33)$$

We can also extend BLL from a single duration  $t$  to an interval by computing the integrated BLL using

$$IBLL = \frac{1}{t_2 - t_1} \int_{t_1}^{t_2} BLL(s) ds. \quad (34)$$

*Belief prediction interval (BPI)* In this paper, we also use the BPIs defined in [11] to evaluate the calibration of the predictive model and, therefore, to understand the reliability of the model's predictions. BPIs are intervals centered at the most plausibility event time

$\mu(x)$  with the degree of belief  $\alpha$  to contain the true value of the response variable, such that  $Bel_{\tilde{Y}(x)}(\mathcal{B}_\alpha(x)) = \alpha, \forall \alpha \in (0; 1]$ . The predictions are said to be calibrated if, for all  $\alpha \in (0; 1]$ ,  $\alpha$ -level BPIs have a coverage probability at least equal to  $\alpha$ , i.e.,

$$\forall \alpha \in (0; 1], P_{X,Y}(Y \in \mathcal{B}_\alpha(X)) \geq \alpha. \quad (35)$$

Similar to the probabilistic case, the calibration of evidential predictions can be assessed using a calibration plot. Predictions are considered calibrated if the curve lies above the first diagonal. The closer the curve approaches the first diagonal, the more precise the predictions are.

#### 4.2. Illustrative dataset

We first provide an illustrative example with a simulated survival dataset to show the model’s robustness to data censoring, as well as study the quantified uncertainties and its calibration to predictions.

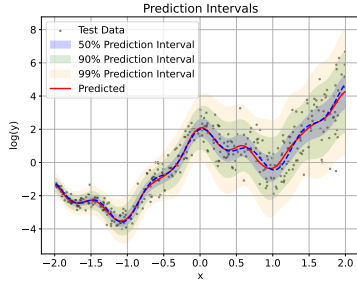
##### 4.2.1. Robustness to data censoring

As shown in Figure 2, the transformed observations  $y = \log(t)$ , the network outputs  $\mu(x)$ , along with belief prediction intervals (BPIs) at levels  $\alpha \in \{0.5, 0.9, 0.99\}$  under 0%, 50%, and 90% censoring rate are presented. When no observations are censored, our model predicts a time-to-event function (red line) that is very close to the ground truth function (blue broken line), and the predicted BPIs effectively encompass all of the data points, as shown in Figure. 2a. When 50% of the observations are censored (Figure 2d), our model is able to predict a survival function that closely aligns with the ground truth. Although there is an upward bias in the predicted function compared to the true sample distribution when data is sparse, the overall predicted curve is still promising. When 90% of the observations are censored (Figure. 2g), the predicted function becomes smoother with fewer details and exhibits an obvious upward bias relative to the true sample distribution, as expected. Nevertheless, the BPIs still effectively encompass the majority of observations, even though the observations are highly censored and far away from the distribution.

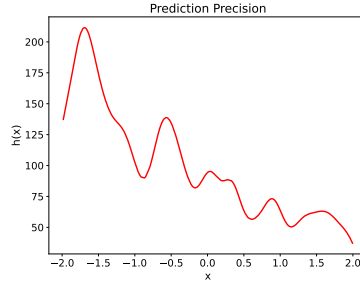
##### 4.2.2. Uncertainty quantification

Data censoring is directly correlated with the randomness of the data, which, in turn, limits prediction precision. A good uncertainty quantification model is expected to effectively capture both the data randomness and prediction precision under varying censoring conditions. As previously mentioned, in addition to predicting the most plausible event time, our model provides two more uncertainty-related information: variance output  $\sigma^2(x)$  and precision output  $h(x)$ . Figure 2c, 2f and 2i show the output standard deviation  $\sigma(x)$  vs.  $x$  at censoring rates of 0%, 50%, and 90%, respectively. It well-captured the increasing trend of data randomness with  $x$ , i.e., as the data censoring rate increases, the data exhibits greater aleatory uncertainty, which, therefore, provides valuable insights for practical decision-making. Figures 2b, 2e, and 2h illustrate the predictive precision  $h(x)$  vs.  $x$  at censoring rates of 0%, 50%, and 90%, respectively. As expected, when the data censoring rate increases, the model has limited ability to predict event time, therefore leading to reduced precision and increased epistemic uncertainty.

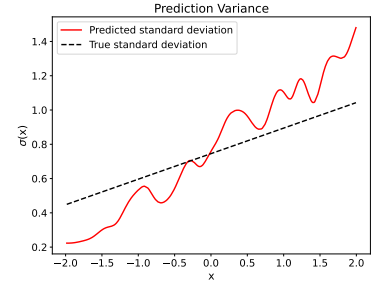
## No data censoring



(a)

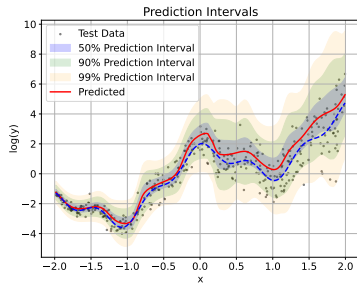


(b)

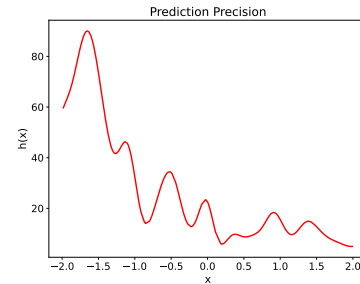


(c)

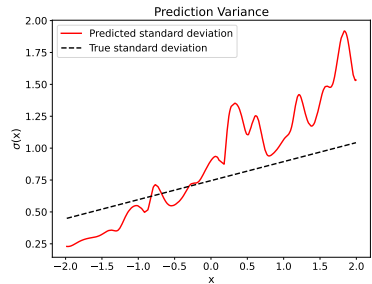
## 50% data censoring



(d)

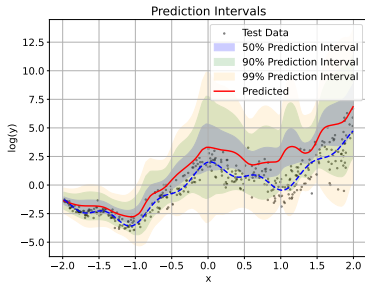


(e)

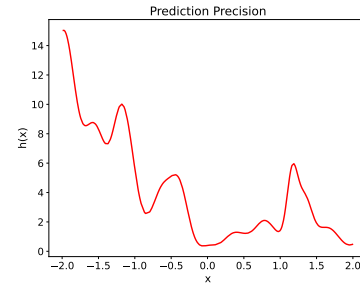


(f)

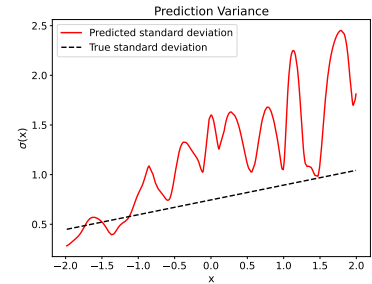
## 90% data censoring



(g)



(h)



(i)

Figure 2: Visualized prediction performance and uncertainty on the illustrative dataset. Figures (a), (d), and (g) show the simulated data, actual regression function (blue broken lines), and predicted function obtained from the trained model (red solid lines) under three censoring rates. Belief prediction intervals (BPIs) at levels  $\alpha \in \{0.5, 0.9, 0.99\}$  are represented by shaded areas in blue, green, and orange. Figures (b), (e), and (h) present the output precision  $h(x)$  under three censoring rates. Figures (c), (f), and (i) present the standard deviation  $\sigma(x)$  under three censoring rates.



#### 4.2.3. Calibration evaluation

In addition to prediction accuracy and uncertainty, we also study the calibration performance of the proposed method to see whether the prediction results are reliable or not. Here we show the reliability diagram in Figure 3 based on the calculated  $\alpha$ -level BPIs (blue line). We also show the calibration plot for the probabilistic prediction intervals defined as  $\mu(x) \pm u_{(1+\alpha)/2}\sigma(x)$  (red line) for comparison. The detailed observations are:

- When no data are censored (Figure 3a), we observed that both prediction intervals are well-calibrated, and the calibration curve of BPIs is close to that of probabilistic prediction intervals, indicating that, for no data censoring, the output precision  $h(x)$  is quite high (confirmed by Figure 2a).
- When 50% of data are censored (Figure 3b), we observed the BPIs are more calibrated compared with the probabilistic ones. While the BPIs are far from the probabilistic ones compared with no data censoring, indicating lower output precision  $h(x)$  (confirmed by Figure 2d). We also observed that the BPIs are more conservative than the probabilistic ones.
- When data is highly censored, e.g., 90% censoring (Figure 3c), we observed that both prediction intervals are not calibrated while BPIs show better calibration performance. Moreover, the BPIs and probabilistic ones are far from each other, which indicates that, for high censoring conditions, the output precision  $h(x)$  is quite low, as expected (confirmed by Figure 2g).

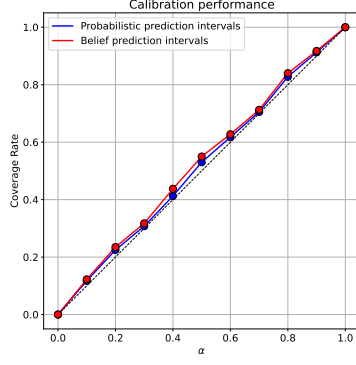
A nice attribute of using GRFNs is that we can do prediction calibration based on the output precision  $h(x)$ . For uncalibrated outputs, we can multiply a constant value  $c$  with the output prediction  $h(x)$  to calibrate the output. For example, we can make the BPIs less conservative by multiplying the output precisions  $h(x)$  by some constant  $c > 1$  or make it more conservative by a constant  $c < 1$ . The probabilistic intervals are recovered when  $c \rightarrow +\infty$ . Figures 3d, 3e and 3f show the reliability diagrams of our model after prediction calibration under censoring rates of 0%, 50%, and 90%, respectively.

#### 4.3. Comparative results on simulated datasets

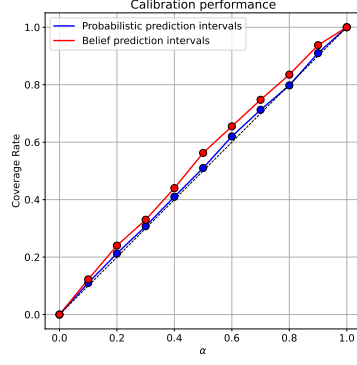
The second experiment focuses on demonstrating the applicability and generalizability of our methods under different data distributions.

*Performance comparison.* As shown in Figure 4, and as expected, the prediction performance is consistently strong when the function of the prediction model aligns with the correct data distribution. For example, the Cox model achieves promising  $C_{idx}$  when the simulated data follows exactly the LPH condition. While in many applications, we cannot assume the data satisfies the linear proportional hazards condition. We then relax the model’s assumption from a linear to a nonlinear form, such as adding an MLP layer to Cox, and the results show that the nonlinear PH models (MLP-Cox) tend to outperform the baseline LPH model (Cox) with more complex data distribution assumptions. Moreover, by further relaxing the hazard assumption from proportional to non-proportional, the results indicate that

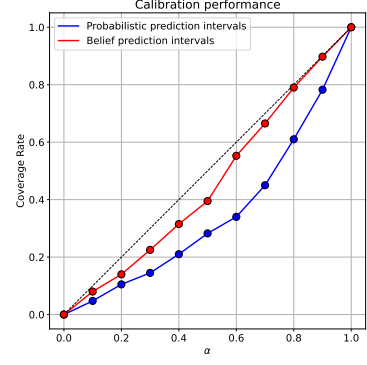
## Orginal Reliability diagrams



(a) No censoring

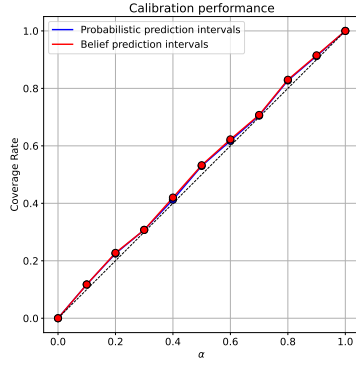


(b) 50% censoring

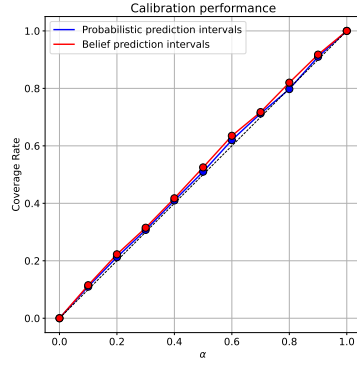


(c) 90% censoring

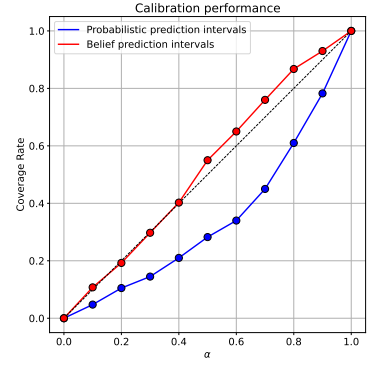
## Reliability diagrams after calibration



(d) No censoring



(e) 50% censoring



(f) 90% censoring

Figure 3: Reliability diagrams for belief prediction intervals (red squares) and probabilistic prediction intervals (blue circles), showing the validation coverage rates vs. the belief or confidence levels  $\alpha \in \{0.1, \dots, 0.9\}$ .

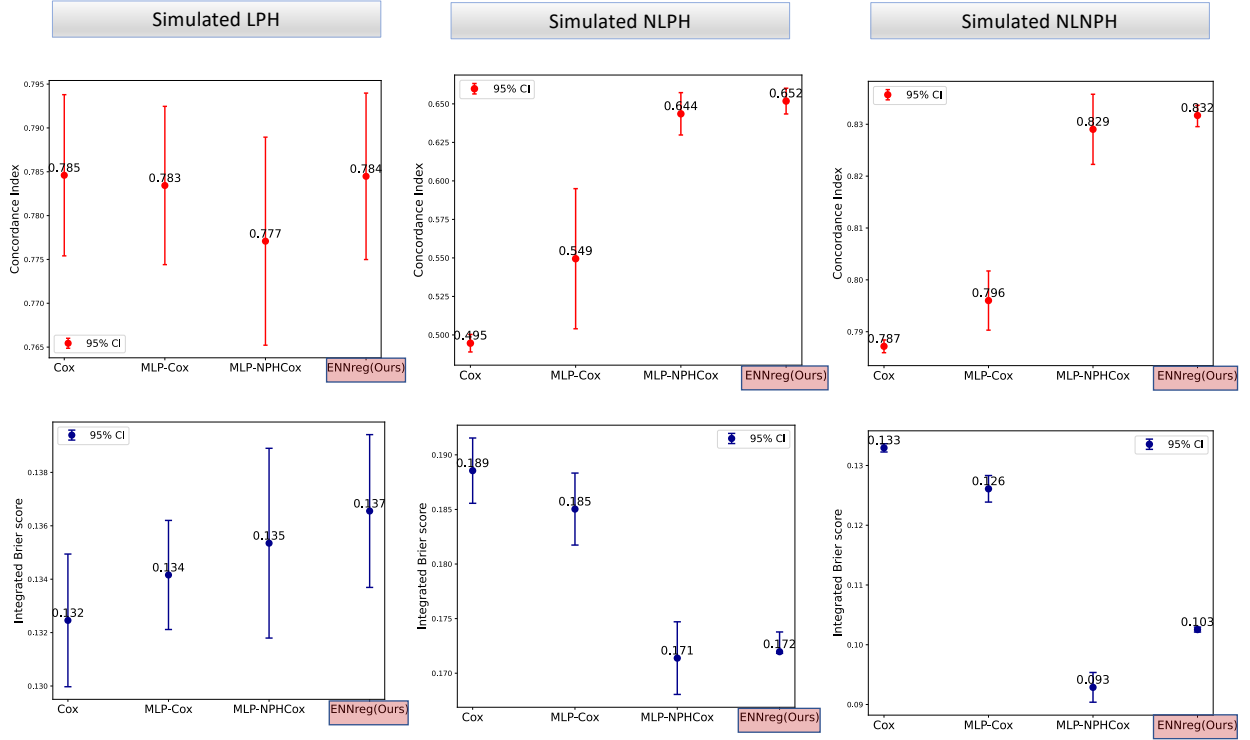


Figure 4: Plots to support the generalizability of our model in different data distributions. The left, middle, and right plots correspond to simulated datasets generated under the LPH, NLPH, and NLNPH assumptions, respectively. In each case, survival prediction is conducted using three models: Cox (holds LPH assumption), MLP-Cox (NLPH assumption), and MLP-NPHCox (NLNPH assumption), alongside our proposed model ENNreg, which predict event time based on GRFNs. These comparisons showcase the robustness of our approach across different distributional assumptions.

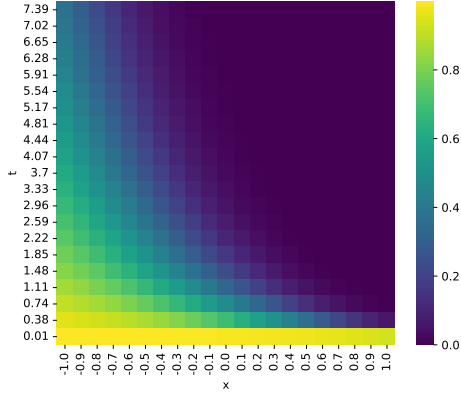
models with stricter assumptions, i.e., Cox and MLP-Cox, have the lowest  $C_{idx}$ . In contrast, the model, MLP-NPHCox, based on more flexible assumptions, which incorporates a non-linear and non-proportional assumption, demonstrates better performance. Nevertheless, in all cases, our model ENNreg using GRFNs to predict event time, consistently achieves either the best or the second-best concordance index, although the differences are not always statistically significant. This demonstrates our model’s ability to flexibly adapt to a wide range of underlying data distribution patterns. The results on the Integrated Brier score also confirmed our conclusion: the prediction performance is more reliable when the prediction model is designed based on the correct data distribution assumption. Nevertheless, our model outperforms others, showing the best overall performance with high  $C_{idx}$  and low IBS.

*Performance Visualization.* Figure 5 demonstrates how ENNreg accurately models the survival function. The first row (Figures 5a, 5c, and 5e) displays the true survival functions under the LPH, NLPH, and NLNPH assumptions, respectively. The second row (Figures 5b, 5d, and 5f) presents the predicted survival functions for these assumptions, respectively. From these figures, it is evident that ENNreg effectively captures both linear and nonlinear relationships between a patient’s covariates  $x$  and their survival function  $y$ . Notably, Figures 5e and 5f demonstrate ENNreg’s superior success in modeling the nonlinear nonproportional conditions with high accuracy.

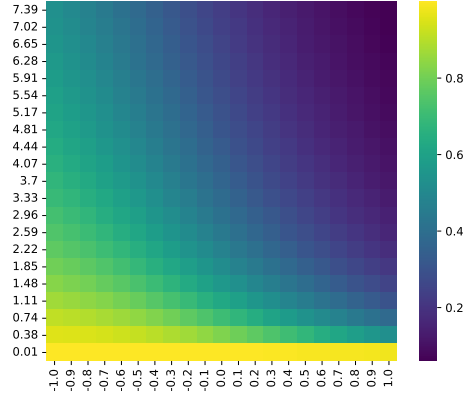
#### 4.4. Comparative results on real-world datasets

The third experiment focuses on demonstrating the applicability and generalizability of our methods in read-word tasks: survival prediction and ICU length of stay prediction. As for the compared methods, Cox is the classical time-to-event model, Deepsurv is the neural network version of the Cox model, and Cox-Time [30] is the time-dependent neural network version of the Cox model. DeepHit [31] is a probability mass function-based discrete-time model with limited data distribution assumption.

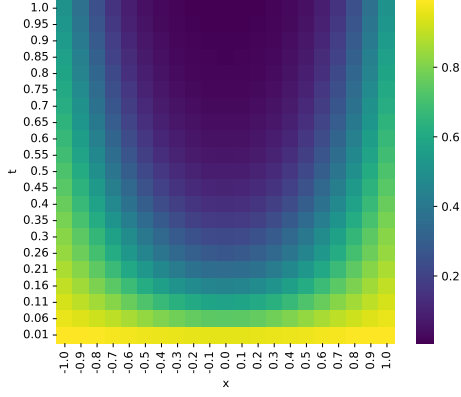
*Comparative results on the survival datasets.* We first consider prediction accuracy. DeepHit shows strong discriminative performance on the  $C_{idx}$  metric compared to the continuous-time models in general. This is not surprising due to the fact that 1) no strong structural assumptions are held for DeepHit; 2) DeepHit has an additional ranking loss tailored for  $C_{idx}$  for parameter optimization. However, our model ENNreg still outperforms Deephit with a higher  $C_{idx}$  and better calibration performance. This result is interesting considering that we did not develop a time-dependent prediction model like Cox-time, nor did we use the concordance index for hyperparameter tuning as in Deephit. We then consider prediction calibration. As we can see from the IBS and IBLI results, the promising concordance performance of Deephit comes at the cost of poorly calibrated survival estimates. In contrast, our proposal exhibits good calibration properties, with statistically significant differences observed in calibrated survival estimates for both datasets.



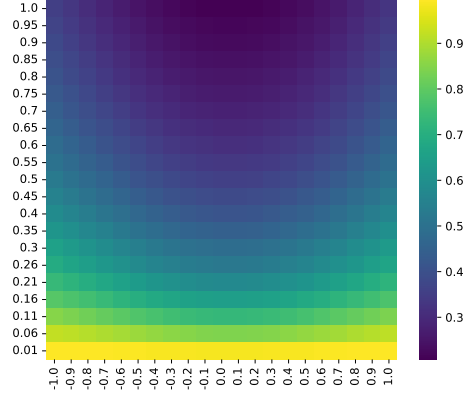
(a) True  $S(t|x)$  of LPH



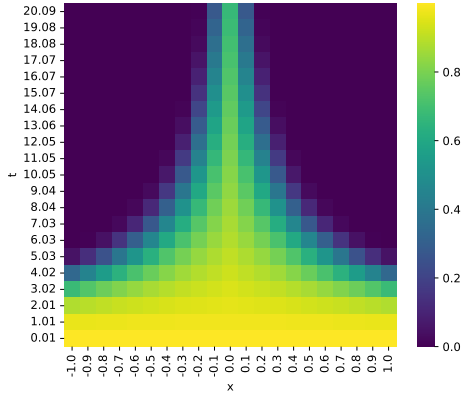
(b) Estimate  $S(t|x)$  of LPH



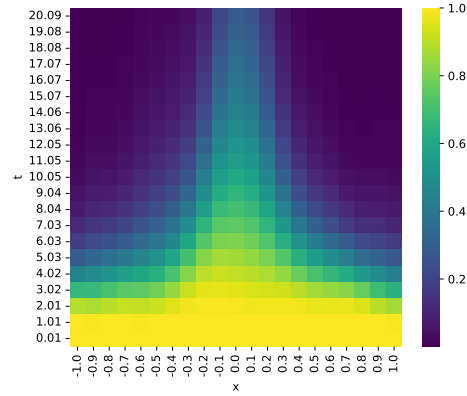
(c) True  $S(t|x)$  of NLPH



(d) Estimate  $S(t|x)$  of NLPH



(e) True  $S(t|x)$  of NLNPH



(f) Estimate  $S(t|x)$  of NLNPH

Figure 5: Survival surfaces  $t$  with respect to patient's covariates  $x$ . The first row of figures displays the true survival surfaces under the LPH, NLPH, and NLNPH assumptions, respectively. The second row displays the predicted survival surfaces for these three assumptions.

Table 2: Comparison of prediction performance (mean and 95% confidence interval (CI)) on three survival datasets. The best and second best results are, resp., in bold and underlined.

Methods	Accuracy (95% CI)	Uncertainty (95% CI)	
	$C_{idx} \uparrow$	IBS $\downarrow$	IBLL $\downarrow$
<b>METABRIC, Size = 1904, censoring rate = 42%</b>			
Cox	0.643 (0.632—0.654)	0.172 (0.169—0.175)	0.515 (0.507—0.522)
Deepsurv	0.503 (0.428—0.576)	0.206 (0.182—0.230)	0.606 (0.544—0.667)
Cox-Time	0.661 (0.651—0.673)	<u>0.165</u> (0.159—0.170)	<b>0.502</b> (0.483—0.521)
DeepHit	<u>0.669</u> (0.649—0.689)	0.180 (0.176—0.183)	0.534 (0.524—0.544)
ENNreg (Ours)	<b>0.672</b> (0.656—0.687)	<b>0.160</b> (0.166—0.171)	<u>0.508</u> (0.502—0.514)
<b>GBSG, Size = 2232, censoring rate = 43%</b>			
Cox	0.662 (0.649—0.675)	0.183 (0.181—0.185)	0.539 (0.534—0.543)
Deepsurv	0.542 (0.456—0.628)	0.202 (0.188—0.215)	0.589 (0.547—0.632)
Cox-Time	0.672 (0.662—0.682)	<u>0.179</u> (0.175—0.183)	<u>0.530</u> (0.518—0.542)
DeepHit	0.667 (0.658—0.676)	0.200 (0.192—0.208)	0.582 (0.552—0.610)
ENNreg (Ours)	<b>0.679</b> (0.670—0.687)	<b>0.178</b> (0.177—0.180)	<b>0.525</b> (0.522—0.528)
<b>SUPPORT, Size = 8873, censoring rate = 32%</b>			
Cox	0.568 (0.564—0.571)	0.204 (0.202—0.206)	0.593 (0.589—0.597)
Deepsurv	0.572 (0.562—0.581)	0.203 (0.200—0.207)	0.593 (0.583—0.602)
Cox-Time	<u>0.610</u> (0.605—0.616)	<u>0.193</u> (0.190—0.196)	<b>0.567</b> (0.561—0.574)
DeepHit	<b>0.626</b> (0.622—0.630)	0.206 (0.205—0.208)	0.600 (0.596—0.604)
ENNreg (Ours)	<b>0.626</b> (0.618—0.634)	0.196 (0.194—0.199)	<u>0.574</u> (0.569—0.580)

Table 3: Comparison of prediction performance (mean and 95% confidence interval (CI)) on the MIMIC-IV datasets. The best and second best results are, resp., in bold and underlined.

MIMIC-IV, Size=53513, censoring rate =89%			
Methods	Accuracy (95% CI)	Uncertainty (95% CI)	
	$C_{idx} \uparrow$	IBS $\downarrow$	IBLL $\downarrow$
Cox	0.779 (0.768-0.790)	0.193 (0.182-0.203)	0.581 (0.544-0.617)
Deepsurv	0.834 (0.826-0.841)	0.220 (0.207-0.233)	0.698 (0.633-0.763)
Cox-Time	<u>0.841</u> (0.834-0.848)	0.193 (0.175-0.210)	0.575 (0.524-0.625)
DeepHit	0.823 (0.813-0.831)	<u>0.184</u> (0.168-0.201)	<u>0.548</u> (0.505-0.590)
ENNreg	<b>0.845</b> (0.837-0.849)	<b>0.190</b> (0.174-0.211)	<b>0.572</b> (0.522-0.625)

*Comparative results on the MIMIC-IV datasets.* Table 3 shows the results of MIMIC compared with SOTA methods. As the data size increases, the advantage of the discrete model DeepHit on the MIMIC dataset diminishes due to information loss. Because the discretization of event times becomes more severe, eventually limiting its discriminative performance. In contrast, continuous prediction models, such as Deepsurv and Cox-time, achieve better prediction accuracy and calibration. Nevertheless, our proposed model, EENNreg, demonstrates the best performance, with the highest  $C_{idx}$  and the lowest IBS and IBLL, showing promising results on large-scale datasets.

We can, therefore, conclude that our evidence-based time-to-event prediction model, based on minimal assumptions, demonstrates greater flexibility and robustness compared to state-of-the-art models that rely on restrictive hypotheses such as the proportional hazard assumption. Aside from accommodating various data distributions, our method can effectively manage different data censoring scenarios, which is confirmed by Fig. 2.

## 5. Conclusion

In this paper, we extended the ENNreg model introduced in [11] to account for censored data, and applied it to time-to-event prediction (called survival prediction as well). This is the first work involving a regression model that can predict the most plausible event time with both aleatory and epistemic uncertainty provided in the presence of data censoring. The model is optimized using an extended negative log-likelihood function that incorporates data censoring, taking the logarithm of the response variable  $T$  as the target variable. The quantified epistemic uncertainty allows us to compute conservative prediction intervals with specified belief degrees with confidence calibration, and the quantified aleatory uncertainty indicates the data quality. Experimental results on simulated datasets with various data distributions and censoring scenarios, as well as on real-world datasets across different clinical settings and tasks, demonstrate that our model consistently achieves both accurate and reliable performance compared to state-of-the-art methods.

This study can be extended in several directions. For complex and large-scale data, a deep feature-extraction module could be used before ENNreg to map input data into deep representative features, resulting in deep evidential neural networks as introduced in [37].

For data from different sources, the fusion of source-depend GRFNs where the uncertain and reliability could be considered as in [22] to achieve more reliable performance. The impact of independence among GRFNs in time-to-event tasks, as introduced in [13], could also be studied. Moreover, the study of mixtures of GFRNs to fit different applications, e.g., finance analysis and climate disaster prediction, can also be considered.

## Acknowledgements

This research is supported by A\*STAR, CISCO Systems (USA) Pte. Ltd, and the National University of Singapore under its Cisco-NUS Accelerated Digital Economy Corporate Laboratory (Award I21001E0002) and the National Research Foundation Singapore under the AI Singapore Programme (Award AISG-GC-2019-001-2B).

## References

- [1] L. Antolini, P. Boracchi, and E. Biganzoli. A time-dependent discrimination index for survival data. *Statistics in medicine*, 24(24):3927–3944, 2005.
- [2] N. E. Breslow. Analysis of survival data under the proportional hazards model. *International Statistical Review/Revue Internationale de Statistique*, pages 45–57, 1975.
- [3] H. Chai, S. Lin, J. Lin, M. He, Y. Yang, Y. OuYang, and H. Zhao. An uncertainty-based interpretable deep learning framework for predicting breast cancer outcome. *BMC bioinformatics*, 25(1):88, 2024.
- [4] P. Chapfuwa, C. Tao, C. Li, I. Khan, K. J. Chandross, M. J. Pencina, L. Carin, and R. Henao. Calibration and uncertainty in neural time-to-event modeling. *IEEE transactions on neural networks and learning systems*, 34(4):1666–1680, 2020.
- [5] D. R. Cox. Regression models and life-tables. *Journal of the Royal Statistical Society: Series B (Methodological)*, 34(2):187–202, 1972.
- [6] A. P. Dawid. The well-calibrated bayesian. *Journal of the American Statistical Association*, 77(379):605–610, 1982.
- [7] A. P. Dempster. Upper and lower probabilities induced by a multivalued mapping. *Annals of Mathematical Statistics*, 38:325–339, 1967.
- [8] T. Denœux. Belief functions induced by random fuzzy sets: A general framework for representing uncertain and fuzzy evidence. *Fuzzy Sets and Systems*, 424:63–91, 2021.
- [9] T. Denœux. An evidential neural network model for regression based on random fuzzy numbers. In S. Le Hégarat-Masclé, I. Bloch, and E. Aldea, editors, *Belief Functions: Theory and Applications*, pages 57–66, Cham, 2022. Springer International Publishing.
- [10] T. Denœux. Parametric families of continuous belief functions based on generalized gaussian random fuzzy numbers. *Fuzzy Sets and Systems*, 471:108679, 2023.
- [11] T. Denœux. Quantifying prediction uncertainty in regression using random fuzzy sets: the ennreg model. *IEEE Transactions on Fuzzy Systems*, 2023.
- [12] T. Denœux. Reasoning with fuzzy and uncertain evidence using epistemic random fuzzy sets: General framework and practical models. *Fuzzy Sets and Systems*, 453:1–36, 2023.
- [13] T. Denœux. Combination of dependent and partially reliable gaussian random fuzzy numbers. *Information Sciences*, 681:121208, 2024.
- [14] T. Denœux. Uncertainty quantification in logistic regression using random fuzzy sets and belief functions. *International Journal of Approximate Reasoning*, 168:109159, 2024.
- [15] D. Faraggi and R. Simon. A neural network model for survival data. *Statistics in medicine*, 14(1):73–82, 1995.
- [16] T. S. Genders, E. W. Steyerberg, H. Alkadhi, S. Leschka, L. Desbiolles, K. Nieman, T. W. Galema, W. B. Meijboom, N. R. Mollet, P. J. de Feyter, et al. A clinical prediction rule for the diagnosis of



- coronary artery disease: validation, updating, and extension. *European heart journal*, 32(11):1316–1330, 2011.
- [17] E. Graf, C. Schmoor, W. Sauerbrei, and M. Schumacher. Assessment and comparison of prognostic classification schemes for survival data. *Statistics in medicine*, 18(17-18):2529–2545, 1999.
  - [18] B. Györfy, A. Lanczky, A. C. Eklund, C. Denkert, J. Budczies, Q. Li, and Z. Szallasi. An online survival analysis tool to rapidly assess the effect of 22,277 genes on breast cancer prognosis using microarray data of 1,809 patients. *Breast cancer research and treatment*, 123:725–731, 2010.
  - [19] F. E. Harrell, R. M. Califf, D. B. Pryor, K. L. Lee, and R. A. Rosati. Evaluating the yield of medical tests. *Jama*, 247(18):2543–2546, 1982.
  - [20] T. Herold, M. Rothenberg-Thurley, V. V. Grunwald, H. Janke, D. Goerlich, M. C. Sauerland, N. P. Konstandin, A. Dufour, S. Schneider, M. Neusser, et al. Validation and refinement of the revised 2017 european leukemianet genetic risk stratification of acute myeloid leukemia. *Leukemia*, 34(12):3161–3172, 2020.
  - [21] L. Huang, S. Ruan, P. Decazes, and T. Denoeux. Deep evidential fusion with uncertainty quantification and contextual discounting for multimodal medical image segmentation. *arXiv preprint arXiv:2309.05919*, 2023.
  - [22] L. Huang, S. Ruan, P. Decazes, and T. Denœux. Deep evidential fusion with uncertainty quantification and reliability learning for multimodal medical image segmentation. *Information Fusion*, 113:102648, 2025.
  - [23] L. Huang, S. Ruan, and T. Denœux. Application of belief functions to medical image segmentation: A review. *Information fusion*, 91:737–756, 2023.
  - [24] L. Huang, S. Ruan, Y. Xing, and M. Feng. A review of uncertainty quantification in medical image analysis: probabilistic and non-probabilistic methods. *Medical Image Analysis*, page 103223, 2024.
  - [25] L. Huang, Y. Xing, T. Denoeux, and M. Feng. An evidential time-to-event prediction model based on gaussian random fuzzy numbers. In *International Conference on Belief Functions*, pages 49–57. Springer, 2024.
  - [26] H. Ishwaran, U. B. Kogalur, E. H. Blackstone, and M. S. Lauer. Random survival forests. *Annals of Applied Statistics*, 2(2):841–860, 2008.
  - [27] A. Johnson, L. Bulgarelli, T. Pollard, S. Horng, L. A. Celi, and R. Mark. Mimic-iv. *PhysioNet*. Available online at: <https://physionet.org/content/mimiciv/1.0/> (accessed August 23, 2021), pages 49–55, 2020.
  - [28] E. L. Kaplan and P. Meier. Nonparametric estimation from incomplete observations. *Journal of the American statistical association*, 53(282):457–481, 1958.
  - [29] J. L. Katzman, U. Shaham, A. Cloninger, J. Bates, T. Jiang, and Y. Kluger. Deepsurv: personalized treatment recommender system using a cox proportional hazards deep neural network. *BMC medical research methodology*, 18(1):1–12, 2018.
  - [30] H. Kvamme, Ø. Borgan, and I. Scheel. Time-to-event prediction with neural networks and cox regression. *Journal of machine learning research*, 20(129):1–30, 2019.
  - [31] C. Lee, W. Zame, J. Yoon, and M. Van Der Schaar. Deephit: A deep learning approach to survival analysis with competing risks. In *Proceedings of the AAAI conference on artificial intelligence*, volume 32, 2018.
  - [32] G. Li, L. Yang, C.-G. Lee, X. Wang, and M. Rong. A bayesian deep learning rul framework integrating epistemic and aleatoric uncertainties. *IEEE Transactions on Industrial Electronics*, 68(9):8829–8841, 2020.
  - [33] C. Lian, S. Ruan, T. Denœux, H. Li, and P. Vera. Joint tumor segmentation in pet-ct images using co-clustering and fusion based on belief functions. *IEEE Transactions on Image Processing*, 28(2):755–766, 2018.
  - [34] A. Mehrtash, W. M. Wells, C. M. Tempny, P. Abolmaesumi, and T. Kapur. Confidence calibration and predictive uncertainty estimation for deep medical image segmentation. *IEEE transactions on medical imaging*, 39(12):3868–3878, 2020.
  - [35] S. Purushotham, C. Meng, Z. Che, and Y. Liu. Benchmarking deep learning models on large healthcare datasets. *Journal of biomedical informatics*, 83:112–134, 2018.

- [36] G. Shafer. *A mathematical theory of evidence*, volume 42. Princeton university press, 1976.
- [37] Z. Tong, P. Xu, and T. Denoeux. An evidential classifier based on dempster-shafer theory and deep learning. *Neurocomputing*, 450:275–293, 2021.
- [38] B. Vinzamuri, Y. Li, and C. K. Reddy. Pre-processing censored survival data using inverse covariance matrix based calibration. *IEEE Transactions on Knowledge and Data Engineering*, 29(10):2111–2124, 2017.
- [39] P. Xu, F. Davoine, H. Zha, and T. Denoeux. Evidential calibration of binary svm classifiers. *International Journal of Approximate Reasoning*, 72:55–70, 2016.
- [40] L. A. Zadeh. Fuzzy sets as a basis for a theory of possibility. *Fuzzy sets and systems*, 1(1):3–28, 1978.
- [41] Q. Zhang and M. Zhou. Nonparametric bayesian lomax delegate racing for survival analysis with competing risks. *Advances in Neural Information Processing Systems*, 31, 2018.
- [42] W.-Z. Zhong, Q. Wang, W.-M. Mao, S.-T. Xu, L. Wu, Y.-C. Wei, Y.-Y. Liu, C. Chen, Y. Cheng, R. Yin, et al. Gefitinib versus vinorelbine plus cisplatin as adjuvant treatment for stage ii-iiia (n1-n2) egfr-mutant nscl: final overall survival analysis of ctong1104 phase iii trial. *Journal of clinical oncology*, 39(7):713, 2021.